Published in final edited form as:
Neuroimage. 2008 January 1; 39(1): 146–156.

A Bayesian Hierarchical Framework for Spatial Modeling of fMRI Data

F. DuBois Bowman[*], **Brian Caffo**[†], **Susan Spear Bassett**[‡], and **Clinton Kilts**[§]

[*]*Department of Biostatistics, The Rollins School of Public Health, Emory University*

[†]*Department of Biostatistics, Johns Hopkins Bloomberg School of Public Health*

[‡]*Department of Psychiatry and Behavioral Sciences, Johns Hopkins Medical Institutions*

[§]*Department of Psychiatry and Behavioral Sciences, School of Medicine, Emory University*

Abstract

Applications of functional magnetic resonance imaging (fMRI) have provided novel insights into the neuropathophysiology of major psychiatric, neurological, and substance abuse disorders and their treatments. Modern activation studies often compare localized task-induced changes in brain activity between experimental groups. Complementary approaches consider the ensemble of voxels constituting an anatomically defined region of interest (ROI) or summary statistics, such as means or quantiles, of the ROI. In this work we present a Bayesian extension of voxel-level analyses that offers several notable benefits. Among these, it combines whole-brain voxel-by-voxel modeling and ROI analyses within a unified framework. Secondly, an unstructured variance/covariance matrix for regional mean parameters allows for the study of inter-regional (long-range) correlations, and the model employs an exchangeable correlation structure to capture intra-regional (short-range) correlations. Estimation is performed using Markov Chain Monte Carlo (MCMC) techniques implemented via Gibbs sampling. We apply our Bayesian hierarchical model to two novel fMRI data sets: one considering inhibitory control in cocaine-dependent men and the second considering verbal memory in subjects at high risk for Alzheimer's disease.

Keywords

functional neuroimaging; Bayesian analysis; connectivity; MCMC; regions of interest; volumes of interest

1 Introduction

Functional neuroimaging techniques enable *in vivo* investigations into the neural basis of human cognition, emotions, and behaviors. In practice, applications of functional magnetic resonance imaging (fMRI) have provided insights into the pathogenesis and pathophysiology of major psychiatric, neurologic, and substance abuse disorders, as well as the neural responses to their treatments. Depending on objectives, fMRI experiments are often employed to study activation or functional connectivity. Activation studies seek to characterize the magnitude and volume of neural responses to experimental tasks by detecting differences in patterns of brain activity between various experimental conditions, between different subgroups of subjects, or

between two or more scanning sessions. In contrast, functional connectivity studies seek to identify areas of the brain that share similar temporal task-related neural responses. We consider a variant of this concept by targeting brain regions that exhibit spatial correlations between summary statistics of the blood oxygen level-dependent (BOLD) neural response profiles, such as task-specific mean effects. These spatial correlations are interpretable as task-related functional connections. We develop a common statistical framework that simultaneously considers activation and task-related functional connectivity. Of note, the model incorporates both long-range and short-range task-related connectivity.

We build on the conventional two-stage approach applied in activation studies for fMRI data. This approach considers individualized voxel-specific time series models in the first stage and voxel-specific population- or group-level models at the second stage (Worsley et al., 2002). In this manuscript, we principally focus on the second stage modeling. The typical voxel-by-voxel second stage regression analyses address spatial correlations by a process of smoothing and Markovian assumptions on resulting statistical maps. We instead focus on both short-range and long-range correlations and formal estimation in a comprehensive statistical model.

Specifically, we develop a spatial Bayesian hierarchical model that is applicable for making inferences regarding task-related changes in brain activity and that identifies and accounts for prominent task-related connectivity. This multilevel model is estimated using Markov chain Monte Carlo (MCMC) techniques. Our Bayesian method offers inferential advantages by providing samples from the joint posterior probability distribution for all of the model parameters, rather than p-values, providing greater flexibility in the inferences that may be drawn from a functional neuroimaging study. Furthermore, our proposed spatial model extends the assumptions underlying previously applied methods and establishes a novel unified framework for voxel-specific and regional (or region of interest (ROI)) inferences, which also uncovers prominent task-related functional connections between remote voxels.

Below, we discuss relevant literature before presenting the proposed Bayesian hierarchical model, estimation procedures, and applications of our model to experimental data from two fMRI studies.

2 Literature review

There is emerging recognition of the importance of modeling correlations between voxels both for estimation and inferences. Some investigators attempt to capture correlations between the measured brain activity in a given voxel with the activity in neighboring voxels. For example, Katanoda et al. (2002) address spatial correlations by incorporating the time series from neighboring (physically contiguous) voxels. Similarly, Gössl et al. (2001) and Woolrich et al. (2004a) consider correlations between neighboring voxels using a conditional autoregressive (CAR) model in a Bayesian framework. Penny et al. (2005) present a Bayesian model that assumes prior distributions with spatial correlations between regression coefficients. They consider first-order neighbors and assume that the covariance matrix is known up to a multiplicative constant.

Other authors extend spatial modeling beyond a localized neighborhood by simplifying the structure of the data. For example, Worsley et al. (1991) present a quadratic decay spatial correlation model for PET data from a selected number of anatomical regions, rather than voxels, significantly reducing the data and the dimensions of the correlation matrix. In a related application, Albert and McShane (1995) present a generalized estimating equations approach for spatially correlated binary data from a study of brain lesions, with a relatively small number (e.g. 88) of spatial locations in each slice. Bowman (2007) considers data from a defined ROI and presents a spatio-temporal model that specifies spatial correlations based on a functionally defined distance metric. In this model, the magnitude of correlations decay as a function of

decreasing similarity, rather than simply as a function of increasing physical distance, allowing the possibility of long-range correlations due, for example, to white-matter axonal connections.

Bowman (2005) presents a whole-brain spatio-temporal model that partitions voxels into functionally related networks and applies a spatial simultaneous autoregressive model to capture intra-regional correlations between voxels with the key practical advantage of fast estimation. Woolrich et al. (2004b) propose a Bayesian modeling framework for fMRI data allowing both separable and nonseparable spatio-temporal models.

As an alternative to modeling spatial correlations, one may indirectly address non-independence between voxels by initially smoothing the data, performing separate univariate analyses at each voxel, and then applying random field theory to determine statistical significance for the entire set of voxels, which makes assumptions about spatial dependencies between voxels (Worsley et al., 1992; Worsley, 1994). The random field theory approach to hypothesis testing links voxel-wise statistics, generally by assuming a stationary or isotropic random field, but it does not directly estimate spatial covariances. Holmes et al. (1996) outlines several issues with the random field approach, including low degrees of freedom to support the theory, noisy statistic images, a questionable assumption of constant error variance across an entire image, and initial spatial smoothing of the data.

The spatial modeling approaches of Katanoda et al. (2002), Gössl et al. (2001), and Woolrich et al. (2004a) provide local smoothing, but limiting spatial associations to a very restricted area (e.g. consisting of contiguous voxels) departs from our current knowledge regarding neurophysiology including functional networks that are spatially disperse (e.g. the visual system). Broca's area and Wernicke's area are specific examples of two noncontiguous anatomical regions that may exhibit long range correlations, given their joint involvement in many language related tasks (Matsumoto et al., 2004). Bowman (2007) demonstrates that a relatively distant pair of voxels may exhibit high positive correlations, even when compared to a more proximal pair of voxels. Local spatial models disregard the possibility of such long-range correlations. Although the approach of Penny et al. (2005) is capable of extending the localized region, it makes an assumption of a known local spatial kernel, rather than estimating all of the variances and spatial covariances from the data.

Considering a coarsened data structure, such as the methods of Worsley et al. (1991) and Albert and McShane (1995), simplifies computations, but sacrifices the potential for localization using fMRI (or PET) data. Bowman (2005) frames a spatial model within a simplified data structure by modeling intra-regional correlations. While this method may incorporate long-range spatial correlations and provides inferences at a refined voxel level as well as broader regional levels, it suffers from the assumption that inter-region voxel pairs are uncorrelated. In contrast to the computationally efficient method of Bowman (2005), the approaches by Woolrich et al. (2004a), Gössl et al. (2001), and Bowman (2007) require extensive computations. Consequently, these methods are less practical due to the long computation times or are limited to small or moderate anatomic regions. For example, Bowman (2007) only considers analyses for ROI's, such as the cerebellum, and the method of Woolrich et al. (2004a) takes roughly 6 hours to analyze data from a single slice.

3 Experimental fMRI data

In this manuscript we highlight the analysis of two novel fMRI data sets that motivated the developed model and represent good examples of its utility. Below we briefly describe each in turn before introducing the model.

The first experiment considers inhibitory control in cocaine-dependent men. Impairments in inhibitory control over drug related behaviors are common characteristics of addicts (Kalivas

and Volkow, 2005). We consider an fMRI study that evaluates the impact of cocaine addiction and treatment-related cocaine abstinence on neural representations of motor inhibition tasks targeting prepotent response inhibition.

Data are available for 15 cocaine-dependent men who received an intensive outpatient behavioral therapy program and did not relapse. Pre and post-treatment scans were taken, with the follow-up scans occurring roughly 24 days after the initial image acquisition. Baseline and follow-up scans are also available for 17 control subjects, matched to the clinical sample on age, race, gender, handedness, education, and early life adversity.

The task involves repeated presentations of visual Go stimuli (uppercase alphabetical letters), appearing for 500 milliseconds (ms) with an inter-stimulus interval of 2.3 seconds. Subjects execute the task by pressing a button as quickly as possible in response to the Go stimulus. A Stop signal, an auditory tone (at 1,000 Hz), lasting 500 ms, occurs at random in 16% of the trials. The presentation of the Stop signal following a Go stimulus is an indicator to the subject to attempt to refrain from executing the Go response.

A Siemens 3 T MR scanner was used to acquire T_2-weighted scans with BOLD contrast. We acquired 30 axial slices (no gap), 3 millimeters (mm) in thickness (repetition time 2.02 seconds, echo time 28 ms, 64×64 array, and a flip angle of 90 degrees).

The second fMRI experiment compares neural activity in subjects at high familial risk for Alzheimer's disease to control subjects during an auditory word-pair-associate task. The task, developed by Bookheimer et al. (2000), was chosen for its role as a processing demand for the medial temporal lobe (MTL), as the MTL is often indicated as an early site of neuropathological changes associated with Alzheimer's disease. The auditory task consists of a memory “encode” phase, whereby subjects are presented unrelated word pairs in a block and a “recall” block, where subjects are asked to recall the second word of the pair when presented with the first. The paradigm included two six minute sessions, each consisting of seven unique word-pairs.

In this manuscript, we consider a follow-up study on the same group of individuals investigated in Bassett et al. (2006) using the same experimental paradigm. We focus only on comparisons of the encode blocks to resting state. Notably, this study included nearly 80 subjects in each group, and limited the image acquisition to a small axial volume surrounding the MTL. As such, the study offers unique data for investigating correlations between regions of interest.

The scans were acquired on a 1.5 T Philips Intera-NT scanner (Philips Medical Systems, Best, The Netherlands). A standard head coil was used to limit head motion. Functional scans were acquired using a BOLD technique with a repetition time of 1000 ms, an echo time of 39 ms, a flip angle of 90 degrees, a field of view of 230 mm in the xy plane and matrix size of 64 × 64 reconstructed to 128 × 128. Eighteen coronal slices were acquired with a 4.5 mm thickness and an interslice gap of 0.5 mm. As the scanning protocol was identical for the second wave, further details on the study and patient group can be found in Bassett et al. (2006).

All subjects in both experiments provided written consent and the studies were approved by the respective Institutional Review Boards.

4 A hierarchical model for functional neuroimaging data

We formulate a model that builds on the conventional two-stage modeling approach for fMRI data that emulates a random effects analysis. Our model captures temporal correlations via the approximate random effects structure and also by addressing serial dependencies between each subject's repeated measurements (Worsley et al., 2002). We then extend the conventional approach by fitting a spatial Bayesian hierarchical model at the second stage, where we capture

correlations in BOLD effects between voxels within defined neuroanatomical structures as well as between different anatomical regions. Incorporating spatial correlations into our statistical model allows us to quantify and make inferences about task-related functional connections between intra-regional voxels and between defined anatomical nodes (regions).

4.1 Stage I: general linear model with serially correlated errors

In light of our two fMRI data examples examining response inhibition among cocaine-dependent men and verbal memory for subjects at-risk for Alzheimer's disease, we present the Stage I model initially for an fMRI study. However, the general framework that we present is also applicable to PET regional cerebral blood flow (rCBF) studies, and one may consider a range of substantive applications that seek to identify localized regions of significant task-related (or between-group) changes in measured brain activity. The first-stage of our approach resembles a general linear model (GLM) for each individual's vector of serial responses at the voxel level (Friston et al., 1995). To set notation, let $i = 1, \ldots, K_j$ index subjects, $s = 1, \ldots, S$ represent scans, and $v = 1, \ldots, V$ index voxels. We arrange the serial fMRI BOLD responses for subject i, measured at voxel v, in the $S \times 1$ vector $\mathbf{Y}_i(v)$. The $S \times q$ design matrix $\mathbf{X}_{iv}$ includes independent variables of interests such as experimental conditions, and $\mathbf{H}_{iv}$ contains covariates that are not of substantive interest, e.g. including a high-pass filtering matrix used to remove unwanted low-frequency trends from the data. For fMRI analyses, we convolve the design matrix with a prespecified hemodynamic response function.

We specify the first-stage model as follows:

$$\mathbf{Y}_i(v) = \mathbf{X}_{iv}\beta_i(v) + \mathbf{H}_{iv}\nu_i(v) + \epsilon_i(v), \quad (1)$$

where $\boldsymbol{\beta}_i(v) = \{\beta_{i1}(v), \ldots, \beta_{iq}(v)\}'$ and $\beta_{ij}(v)$ is the effect corresponding to stimulus j (for subject i), $\boldsymbol{\nu}_i(v)$ includes parameters associated with $\mathbf{H}_{iv}$, and the mean-zero vectors of random errors $\boldsymbol{\epsilon}_i(v)$ are independent and follow a multivariate normal distribution with variance $\mathrm{Var}\{\epsilon_i(v)\} = \tau_v^2\mathbf{V}$. The matrix $\mathbf{V}$ specifies the serial correlations in the data. We fit the first-stage model using SPM2, which accounts for serial correlations using a linear covariance model for $\mathbf{V}$, consisting of a first-order autoregressive component plus white noise (Kiebel, 2003). The associated covariance parameters are estimated using restricted maximum likelihood (REML). Alternative estimation procedures such as the Cochrane-Orcutt method (Worsley et al., 2002) and the expectation-maximization (EM) algorithm (Friston et al., 2002) are also available.

4.2 Stage II: spatial Bayesian hierarchical model

We consider an anatomical parcellation of the brain consisting of $g = 1, \ldots, G$ regions, where we may set G as high as 116 (Tzourio-Mazoyer et al., 2002). Alternative anatomical parcellations are also available, such as those based on Brodmann regions (Garey, 1994) or on tools by Fischl et al. (2004, 2002) implemented in the Freesurfer software. Let V_g represent the number of voxels in a particular region indexed by g. We then denote the individualized Stage I regression estimate (from Equation 1) of the fMRI BOLD response vector associated with stimulus j by $\boldsymbol{\beta}_{igj} = \{\beta_{igj}(1), \ldots, \beta_{igj}(V_g)'$. Here, we slightly modify our earlier notation by collecting localized effects from all voxels in region g into a single vector.

Our Stage II model has the following hierarchical structure:

$$\begin{aligned}
\beta_{igj}|\mu_{gj},\alpha_{igj},\sigma^2_{gj} &\sim \text{Normal}\left(\mu_{gj}+1\alpha_{igj},\sigma^2_{gj}\mathbf{I}\right)\\
\mu_{gj}|\lambda^2_{gj} &\sim \text{Normal}\left(1\mu_{0gj},\lambda^2_{gj}\mathbf{I}\right)\\
\sigma^{-2}_{gj} &\sim \text{Gamma}\,(a_0,b_0)\\
\alpha_{ij}|\Gamma_j &\sim \text{Normal}\left(0,\Gamma_j\right)\\
\lambda^{-2}_{gj} &\sim \text{Gamma}\,(c_0,d_0)\\
\Gamma^{-1}_j &\sim \text{Wishart}\left\{\left(h_0\mathbf{H}_{0j}\right)^{-1},h_0\right\}
\end{aligned} \tag{2}$$

where $\boldsymbol{\mu}_{gj} = (\mu_{gj}(1), \ldots, \mu_{gj}(V_g))'$ and $\boldsymbol{\alpha}_{ij} = (\alpha_{i1j}, \ldots, \alpha_{iGj})'$.

The top level of our hierarchical model specifies a multivariate normal likelihood function for the response vectors, $\boldsymbol{\beta}_{igj}$. For each voxel in region g, $v = 1, \ldots, V_g$, the subject-specific quantities $\beta_{igj}(v)$ are assumed to vary randomly about a mean consisting of both a population-level mean parameter $\mu_{gj}(v)$ and an individualized (random effect) component α_{igj}. Given the random effects parameter, α_{igj}, the covariance matrix of $\boldsymbol{\beta}_{igj}$ is given by $\sigma^2_{gj}\mathbf{I}$. Our model yields a conditional independence assumption, indicating that the spatial correlations between all pairs of voxels within region g are mediated by the random effects parameters.

At the next level, the model expresses a prior belief that each voxel's population mean (for the jth effect) arises from a normal distribution with a mean given by the overall region mean μ_{0gj} and variance λ^2_{gj}. The data will help to inform this prior assumption, but it seems to represent a reasonable starting point to assume that voxels within anatomically-defined regions exhibit task-related activity that deviates around an overall mean for that region. If sufficient prior information is available, we can relax this assumption to accommodate voxel-specific means for the prior parameter vector. At the final level, our hierarchical model captures potential paradigm-related functional connections between anatomical brain regions through the covariance matrix $\boldsymbol{\Gamma}_j$. We provide additional details regarding task-related connectivity in Section 4.3.

In addition to voxel-specific quantities, interest may also lie in regional parameters that pool a collection of voxels in a region $\mathcal{R}_g$. From our model, it is natural to define regional parameters such as the mean regional activation: $\theta_{gj} = \sum_{v\in\mathcal{R}_g} \mu_{gj}(v)/V_g$. Another candidate parameter of interest would consider a specified upper percentile of regional activation. We can easily estimate these and other regional summaries using samples from the joint posterior distribution for all of our model parameters, taking into account the potential correlations between voxel-specific parameters from the region. Partial volume effects (or non-exchangeability) within regions can be addressed by considering regions at different levels of neuroanatomic resolution. If exchangeability of voxels within neuroanatomic regions remains in question, or neuroanatomic regional summaries are not of principal interest, then more data-driven regions (Bowman, 2005) or voxel-wise regression approaches should be used.

4.3 Task-related functional connectivity

Our Bayesian hierarchical model (2) allows us to capture information regarding paradigm-related functional connectivity both within a defined anatomical structure and between brain regions. We use the phrase *task-related functional connectivity* broadly to describe both long- and short-range spatial correlations between task-specific estimates of Stage I BOLD effects, building on the more common use of *functional connectivity* in the fMRI literature to refer to correlations between the BOLD time series from different brain regions. For example, Friston et al. (1993) describes functional connectivity as the correlations between remote neurophysiological events. Our modified concept targets spatial correlations between

paradigm-related neural activity arising from axonal connections and other sources. The short-range correlations reflect neurophysiological associations as well as spatial preprocessing and the intrinsic resolution of the fMRI images. The Bayesian hierarchical model also allows statistical inferences that examine differential task-related functional connectivity between sub-groups.

There have been considerable methodological developments for quantifying functional connectivity, including seed-based approaches (Hampson et al., 2002) that compute correlations between a selected voxel (seed) and other voxels within the brain. Also, Patel et al. (2006a) and Patel et al. (2006b) develop a Bayesian model that targets functional connectivity by identifying voxel pairs that have high joint probabilities of elevated neural activity (above arbitrarily defined levels). By pursuing objectives of activation studies in a framework that accounts for task-related functional connectivity, our proposed method is complementary to and has a much broader scope than these previous works.

Our model captures the short-range task-related connectivity between voxels within a defined anatomical region as well as the (potentially) long-range inter-regional connectivity. We consider the intra-regional connectivity first. Specifically, the first level of the hierarchical model in (2) and the subject- and region-specific random effect, α_{igj}, imply the following conditional exchangeable correlation structure

$$\mathrm{Var}\left(\beta_{igj}|\mu_{gj}\right)=\gamma_{gg}^{(j)}\mathbf{J}+\sigma_{gj}^{2}\mathbf{I},$$

where $\gamma_{gg}^{(j)}$ is gth diagonal element from $\mathbf{\Gamma}_j$. This exchangeable model builds in equal correlations between all pairs of voxels within a defined anatomical region. Specifically,

$$\rho_{gj}^{(\mathrm{w})}=\frac{\gamma_{gg}^{(j)}}{\gamma_{gg}^{(j)}+\sigma_{gj}^{2}}, \tag{3}$$

represents a measure of the strength of task-related intra-regional connectivity. Thus, $\rho_{gj}^{(\mathrm{w})}$ reflects the coherence or the similarity in the paradigm-related neural activity between voxels *within* a given anatomical structure and may vary for different groups, e.g. for patients and controls. One may structure the model to address intra-regional correlations within the same hemisphere or employ an extended model to additionally capture bilateral intra-regional correlations between voxels in separate hemispheres, e.g. the right and left amygdala.

Another component of the paradigm-related functional connectivity is that which occurs between anatomical regions, captured in our framework by the correlations stemming from the covariance matrix, $\mathbf{\Gamma}_j$, of the random effect parameters $\boldsymbol{\alpha}_{ij} = (\alpha_{i1j}, \ldots, \alpha_{iGj})'$. We specify a Wishart prior for $\mathbf{\Gamma}_j^{-1}$, allowing a flexible unstructured covariance matrix. The multivariate structure enables us to compute the inter-regional connectivity matrix (with respect to stimulus j) by

$$\mathbf{R}_j=\left\{\mathrm{Diag}\left(\mathbf{\Gamma}_j\right)\right\}^{-1/2}\quad\mathbf{\Gamma}_j\left\{\mathrm{Diag}\left(\mathbf{\Gamma}_j\right)\right\}^{-1/2}, \tag{4}$$

where the (g_1, g_2) element in $\mathbf{R}_j$ represents the connectivity between anatomical regions g_1 and g_2. More explicitly, the correlations between the estimated BOLD effects from inter-regional voxel pairs, corresponding to regions g_1 and g_2, are given by

$$\rho_{g_1g_2j}^{(\mathrm{b})}=\frac{\gamma_{g_1g_2}^{(j)}}{\sqrt{\left(\gamma_{g_1g_1}^{(j)}+\sigma_{g_1j}^{2}\right)\left(\gamma_{g_2g_2}^{(j)}+\sigma_{g_2j}^{2}\right)}}. \tag{5}$$

4.4 Prior specifications and posterior inference

To complete our Bayesian hierarchical model, we set $a_0 = 0.1$, $b_0 = 0.005$, $c_0 = 0.1$, $d_0 = 0.01$, and $h_0 = G$, resulting in vague or weakly informative priors. The values for a_0, b_0, c_0, and d_0 generate densities that place large probability masses on large variances. The rationale for using these vague priors is to ensure that the information in the data primarily governs the results. However, more informative priors may be employed when fairly precise information is available. Note that the variance parameters were very well estimated in our analyses, and our results were not sensitive to the choice of either diffuse or more informative priors. For example, we also considered the values $a_0 = 2.9$, $b_0 = 0.5$, $c_0 = 2.9$, and $d_0 = 6.4$ in our analysis of the cocaine-dependence data, e.g. giving a theoretical mean $E\left(\sigma_{gj}^2\right) = 1.05$, and the results were essentially identical to those obtained when specifying diffuse or weakly informative priors.

For the inverse-Wishart prior, the degrees of freedom must satisfy $h_0 \geq G$ to yield a proper prior distribution. This prior becomes more diffuse as h_0 gets smaller (West and Harrison, 1989); hence, we set $h_0 = G$ to reflect the most diffuse proper prior that our data can support. A seemingly natural choice for $\mathbf{H}_{0j}$ is a point estimate of $\mathbf{\Gamma}_j$. We use the sample covariance matrix corresponding to the jth effect to obtain $\mathbf{H}_{0j}$, calculated from the subject- and effect-specific mean activity levels in each of the anatomical regions. Note that the use of the sample covariance matrix provides a conservative estimate of the true variation, as it includes both the regional variation, $\gamma_{gg}^{(j)}$, as well as the measurement variation σ_{gj}^2/V_g. We favor this use of a conservative point estimate, to safeguard against under-estimating the variability. In addition, we examine the sensitivity of our results to the sample covariance matrix by artificially reducing the correlations (covariances) using

$$\mathbf{H}_{0j}^{*} = (1 - \omega)\,\mathbf{H}_{0j} + \omega \left\{\mathrm{diag}\left(\mathbf{H}_{0j}\right)\right\}.$$

where $0 \leq \omega \leq 1$. To avoid introducing prior information that does not seem physiologically plausible and that is not supported by the data, we consider small to moderate departures from the sample covariance matrix in our sensitivity analyses. For example, we consider $\omega \in [0, 0.25]$, reflecting up to a 25% decrease in the sample correlation estimates produced by our data.

We implement MCMC methods for estimation using Gibbs sampling. Applying MCMC methods in our context is complicated by the massive amount of data, the vast number of spatial locations, and the large number of parameters. However, the Gibbs-friendly model specification facilitates estimation by providing substantial reductions in computing time and memory.

We present the full conditionals required to run the Gibbs sampler below. To simplify our presentation, let $\mathbf{D}_j^{-1} = \mathrm{diag}\left(V_1\sigma_{1j}^{-2}, \ldots, V_G\sigma_{Gj}^{-2}\right)$, $\bar{\beta}_{gj} = \frac{1}{K_j}\sum_{v=1}^{K_j}\beta_{igj}$, $\bar{\mu} = \left(\bar{\mu}_1, \ldots, \bar{\mu}_{Gj}\right)'$, with $\bar{\mu}_{gj} = \frac{1}{V_g}\sum_{v=1}^{V_g}\mu_{gj}(v)$, and $u_{igj} = \left(\beta_{igj} - \mu_{gj} - 1\alpha_{igj}\right)'\left(\beta_{igj} - \mu_{gj} - 1\alpha_{igj}\right)$. We derive the full conditional distribution for each parameter, that is the distribution of a parameter conditional on all other parameters in the model. The full conditionals are given by the following (we omit notation for conditioned variables for simplicity):

$$
\begin{aligned}
\mu_{gj} &\sim \text{Normal}\left[\Omega_{gj}\left\{\lambda_{gj}^{-2}\mu_{0gj}1+K_j\sigma_{gj}^{-2}\left(\bar{\beta}_{gj}-1\bar{\alpha}_{gj}\right)\right\},\Omega_{gj}\right] \\
\sigma_{gj}^{-2} &\sim \text{Gamma}\left\{a_0+K_jV_g/2,\left(\frac{1}{b_0}+\frac{1}{2}\sum_{i=1}^{K_j}u_{igj}^2\right)^{-1}\right\} \\
\alpha_{ij} &\sim \text{Normal}\left[\Psi_j\left\{\mathbf{D}_j^{-1}\left(\bar{\beta}_{ij}-\bar{\mu}_j\right)\right\},\Psi_j\right] \\
\lambda_{gj}^{-2} &\sim \text{Gamma}\left\{c_0+V_g/2,\left(\frac{1}{d_0}+\frac{(\mu_{gj}-1\mu_{0gj})'(\mu_{gj}-1\mu_{0gj})}{2}\right)^{-1}\right\} \\
\Gamma_j^{-1} &\sim \text{Wishart}\left\{\left(h_0\mathbf{H}_0+\sum_{i=1}^{K_j}\alpha_{ij}\alpha_{ij}'\right)^{-1},h_0+K_j\right\},
\end{aligned}
\tag{6}
$$

where $\Omega_{gj}=\left(\lambda_{gj}^{-2}+K_j\sigma_{gj}^{-2}\right)^{-1}$ $\mathbf{I}$ and $\Psi_j=\left(\Gamma_j^{-1}+\mathbf{D}_j^{-1}\right)^{-1}$.

Iterating through simulations from the full conditionals, updated with the most recent simulated parameters, results in (following a burn-in period) draws from the joint posterior distribution of the parameters. In the examples that follow, we exploit these simulations to perform Bayesian inference on a variety of relevant functions of the parameters. Of particular note for functional neuroimaging analyses, one can easily specify contrasts of mean-level parameters of interest and estimate these quantities from the MCMC joint posterior samples.

5 Results

We apply our Bayesian hierarchical model to both the fMRI study of inhibitory control in cocaine-dependent men as well as to the auditory memory encoding and retrieval study of individuals who are at high risk for developing Alzheimer's disease. We divide our investigations into two sections: mean comparisons (in Section 5.1) and variance components (in Section 5.2). We use the cocaine-dependence data to highlight relevant mean comparisons and the Alzheimer's data to highlight variance components. This stems from the fact that the voxel and regional mean results were more interesting for the cocaine-dependence data and the variance components presented interesting results for the Alzheimer's disease data.

5.1 Voxel-level and regional mean comparisons

First, we consider voxel-specific inferences regarding neural processing alterations related to inhibitory control for cocaine-dependent men before and after intensive behavioral therapy for their addiction. To adjust for learning (or other) effects associated with repeated scanning at baseline and at the follow-up period, we quantify treatment-emergent changes in measured brain activity in the cocaine addicts relative to the corresponding alterations in the healthy control subjects. In summarizing the results from our analysis of the inhibitory control data, we quantify treatment-related changes in brain activity as the post-treatment quantity of interest (e.g. group average within a voxel or within a region) minus the pre-treatment quantity. Similarly, we quantify changes for the control subjects as follow-up estimates minus the baseline estimates.

Figure 1 displays axial slices showing voxels exhibiting treatment-emergent inhibitory control-related changes in neural processing for the cocaine-dependent men that exceed the corresponding changes in the controls, with high probability. The highlighted voxels have posterior probabilities exceeding 0.80 and include the medial orbital frontal cortex (BA 11), the left and right thalamus, left middle frontal gyrus (BA 46), the left and right middle frontal gyrus (BA 9), and the cingulate gyrus (BA 31, 32). The thresholded posterior probability maps reveal voxels for which the data provide evidence of treatment-related increases in the cocaine-dependent men. Statistical inferences may also be targeted using Bayes factors or credible

intervals. Here the 95% credible intervals reveal 719 voxels that have positive lower bounds, providing evidence of treatment-related increases in neural activity for the cocaine-dependent subjects relative to the healthy controls. The voxel-specific effects of treatment indicate the recruitment of thalamo-cortical pathways in attaining the relapse prevention goals of behavioral therapies. Functional inferences include the involvement of alterations in drug valuation and in the mental representation of drug contingencies, facilitation of regulatory control of responses to drug incentives, and the engagement of cognitive control processes related to response conflict monitoring drug availability.

In addition to voxel-level summaries, which are neuroanatomically unconstrained, interest may also lie in quantifying treatment-related neural processing changes for an entire neuroanatomic region. We consider regional mean summaries, noting that summaries over a region typically combines voxels that do and do not demonstrate elevated activity. The number of voxels with elevated activity and the extent of increased activity will determine whether the entire region is declared to show increased activity. In practice, we recommend that voxel-specific analyses accompany region-level investigations to gain a better understanding of the distributed activations within each region underlying the regional summaries. We consider 11 regions that were selected prior to the analysis. For stable estimation of the between-region covariance parameters, the 11 regions were limited to be less than the smallest sample size within any subgroup (e.g. cocaine addicts prior to treatment) and were deemed to be the most relevant to the inhibitory control task.

In the cocaine-dependence data, we evaluate regional treatment-related differences in the neural response to the inhibitory control task by comparing the estimated posterior probabilities that the treatment response in the cocaine addicts exceeds the (learning) response in the control group. The data provide strong evidence of treatment-related increases in inhibitory control-related activity for the cocaine-dependent subjects, relative to the healthy controls, in both the left and right thalamus. The posterior probabilities of treatment-related increases in activity for the cocaine-dependent subjects are both estimated to exceed 0.99, based on the Monte Carlo samples from the posterior distribution. Also, the 95% credible intervals for these regions, estimated from the posterior distribution samples, fall above zero, providing evidence of increased activity associated with treatment for cocaine dependence. The posterior means in these regions for the post- minus pre-treatment differences were at least 0.25 for the cocaine addicts and no greater than 0.07 for the controls. In addition, the data provided moderately strong evidence that the cocaine-dependent subjects exhibited treatment-related increases in neural functioning that exceeded those in the healthy controls in the right pars operculum of the inferior frontal cortex, with an estimated probability of 0.84. However the estimated 95% credible interval for this region included zero.

The results of the region-level analysis suggest the engagement of treatment-emergent, bilateral activations of the thalamic and to a lesser extent frontal cortical regions that correlate to behavioral regulatory functions including attentional, habit suppression and memory retrieval processes necessary to foregoing cocaine use in early abstinence states. Our analysis targets a hypothesis concerning treatment-related neural processing changes associated with response inhibition in cocaine-dependent men, which has not been well-explored in the literature. However, previous research investigating inhibitory control tasks in healthy control subjects or separately in subjects with cocaine dependence has focused on some of the same brain areas identified by our analysis, including the inferior and middle frontal cortex, the cingulate cortex, and subcortical basal ganglia structures including the thalamus (Rubia et al., 2001; Konishi et al., 1999; Garavan et al., 2002; Aron and Poldrack, 2006; Blasi et al., 2006). Although we emphasize the mean-level results here, we note that the maximum inter-regional (posterior median) correlation estimate (0.54) was obtained between the left thalamus and the medial orbito-frontal cortex. This correlation estimate suggests task-related functional connectivity

between these two structures, which are connected by a frontal-subcortical neuroanatomic circuit.

5.2 Regional variance components

The posterior means of $\rho_{gj}^{(w)}$ provide measures of regional coherence or intra-regional task-related functional connectivity. We present results of the intra-regional correlations from the Alzheimer's disease data. There were 46 regions within the imaging area. Though all 46 were considered, areas of the temporal and limbic lobes are of particular interest, having been indicated as having either increased or decreased encoding activity between at-risk subjects and controls in the first wave of the Alzheimer's data or being thought to be involved with the (verbal memory) paradigm (Bassett et al., 2006). Of interest, the large number of subjects allowed for a finer parcellation of regions relative to the cocaine-dependence data.

Table 1 shows the estimates of intra-regional task-related functional connectivity for all of the regions of interest, as well as confidence intervals for the ratio of at-risk subjects to control subjects. The table reveals a high degree of connectivity in the left and right middle temporal and left inferior (orbital) frontal cortex regions. As expected, however, these regions had few voxels. In general, there was a strong, linear negative trend between the number of voxels within a region and the estimated intra-regional functional connectivity, because smaller regions are likely to exhibit a greater degree of coherence in neural activity across voxels.

The 95% credible intervals for the ratio of the correlations between the groups did not overlap one (indicating differential connectivity between groups) in the: left and right anterior cingulate gyrus (CIs of [0.52, 0.92] and [0.47, 0.84], respectively), the left middle cingulate gyrus ([0.53, 0.98]), the pars triangularis of the right inferior frontal cortex ([0.54, 0.96]), and the left superior frontal gyrus ([0.54, 0.92]). It is of interest to note that these regions were sites of differential activation patterns in the first wave of images for this study (Bassett et al., 2006). Also, the control subjects showed significantly lower intra-regional functional connectivity than the at-risk subjects in these cases. This pattern was somewhat persistent; for example, 28 of the 46 posterior mean estimates of these correlations were larger for at-risk subjects.

By considering many regions simultaneously, multiplicity concerns are potentially of interest, though often in likelihood-based analyses, such as the Bayesian one presented here, multiplicity is not addressed (Royall, 2000, 1997; Blume, 2002). It is incorrect to create the credible intervals using a Bonferroni-corrected nominal level, as the credible intervals are not interpreted using frequentist error rates. Instead, one could consider the joint posterior of all regions, though this creates dimensionality concerns. For our application, we alert the reader to consider the results with the caveat that multiplicity was not directly addressed and that such issues are of current research interest (Tadesse et al., 2005). We provide some additional remarks regarding multiplicity in the Discussion section.

5.3 Inter-regional investigations

We now consider inter-regional investigations, considering the group specific correlation matrices, $\mathbf{\Gamma}_j$. Figure 2 shows the posterior means of the correlation matrices for both the control and at-risk subjects for the 46 regions, thresholded at 0.4 for ease of visualization. As expected, the largest degree of inter-regional connectivity was found between bi-lateral regions. For example, among the controls there was a large posterior mean correlation between the left and right caudate (.62), the left and right medial portion of the cingulate gyrus (.67), the left and right middle frontal gyri (.61), and the left and right thalamus (.63). In addition, there was evidence of a large degree of connectivity, with several posterior mean correlations being above .5, within the frontal lobe subregions and cingulate gyrus subregions. The at-risk subjects showed a higher degree of functional correlation, with correlations of .69, .77, .66 and .67 for

the same regions, respectively. Of interest, the correlations within the frontal and cingulate gyri were also higher.

The most striking features of Figure 2 are the overwhelmingly positive correlations between the various regions and an overall pattern of much greater inter-regional functional connectivity among the at-risk group.

To formally compare the inter-regional functional connectivity between the two groups, two omnibus summaries of the variance matrices were used, the ratio of the determinants and greatest root statistic (see Mardia et al., 1979). The ratio of determinants had a 95% credible interval of [1.08, 109.55] while the greatest root statistic had a credible interval of [0.87, .91]. (The greatest root statistic is 1/2 when the two variance matrices are equal.) Both intervals suggest a difference in inter-regional functional connectivity between the at-risk subjects and the controls.

5.4 Implementation notes

The MCMC runs were investigated to ensure the stability of the results. However, the volume of data in question prevents formal use of MCMC convergence tools, such as consistent batch means (Jones et al., 2006). Instead, more informal approaches were taken. Trace plots were used to assess convergence to stationarity for region-specific univariate parameters, such as σ_{gj}. Trace plots for voxel-specific parameters were investigated by taking a small random sample of voxels. All plots suggested rapid convergence to stationarity. For the reported region-level parameters, adhoc batch means methods were employed, with batch sizes determined by informal investigation of the serial autocorrelation in the Markov chain. Typical batch sizes were 100. A small number of burn-in samples (200) were used when starting values appeared in the extreme tails of the stationary density.

The impact of hyper-parameters on results was investigated first by comparing posterior mean estimates with corresponding moment-based estimates and secondly by sensitivity analysis performed by varying the prior parameters with regard to the degree of diffuseness. The impact of the Wishart prior specification was investigated as described in Section 4.4. Starting values were obtained using moment-based estimates. The choice of minimally informative gamma hyper-parameters was guided by comparing the gamma full conditionals to those obtained with the shape set to 0 and the scale set to ∞.

5.5 Validity

In this section, we perform brief simulation studies to investigate the validity of the model. As this model should be viewed as complementary to commonly applied voxel-by-voxel regression analyses, the focus here is to study whether or not the model achieves what it purports to, and whether or not the sample size admits the level of investigation considered.

Because the resulting quantities of principal interest in the cocaine-dependence data are mean-level statistics, while variance and second-level quantities are of primary interest in the Alzheimer's disease data set, we use parameter estimates and sample sizes from those data sets to define two simulation scenarios. The first, based on the cocaine-dependence data, investigates mean-level conclusions. To simulate data, we fix the sample sizes, means, and variances in the hierarchical model at the estimated values obtained from an analysis of the experimental data. Hence, the mean parameters were fixed and not generated. The second fixes only the variance components and sample sizes at the estimated values from the Alzheimer's disease data and simulates from the resulting model. Hence, the means were simulated, while the variances remained fixed.

Our simulation study of the mean-level parameters validate that these quantities are estimated quite accurately. We generated 200 data sets as previously described, estimated model parameters using our hierarchical model, and various measures of accuracy were considered. The mean squared errors for the voxel-specific means for each subject group and treatment period formed empirical distributions that were centered around zero. The parameters for the control group during the follow-up session were estimated most accurately, with first and third quartiles of the mean squared errors given by 0.0007 and 0.0095, respectively. The estimates of the post-treatment parameters for the cocaine-dependent subjects exhibited the highest errors with the first and third quartiles given by 0.0019 and 0.0255, respectively.

From our simulation study of the mean-level parameters, we also investigated the extent to which inferences based on our model would identify voxels that are deemed active or inactive, with respect to the treatment related changes in neural processing associated with the inhibitory control task. This type of analysis requires an arbitrary declaration of which voxels are considered active and those that are deemed inactive. Here, we declared the 2.5% of voxels with the greatest treatment-related changes in neural functioning as *active* and the remaining voxels as *inactive*. Based on these definitions, our model exhibited high sensitivity, with the 95% credible intervals correctly identifying over 90% of the active voxels. Similarly, our model yielded high specificity by correctly classifying 94% of the inactive voxels. Varying the arbitrary threshold defining active and inactive voxels by reducing the number of active voxels, e.g. to 1% by targeting a more restricted subset of the active voxels, increases the sensitivity and decreases the specificity, while classifying less active voxels as active generally reduces the sensitivity and increases the specificity.

For the random effect analysis, three sample sizes were considered, 35, 70 and 140. In all cases the sum of the squared errors for the components of $\mathbf{\Gamma}_j$ decreased (as expected) as the sample size increased, suggesting the validity of the implementation. The square roots of the medians of these aggregated squared errors across simulations were 1.961, 1.955, and 1.942 for $\mathbf{\Gamma}_1$ and 4.600, 4.581 and 4.578 for $\mathbf{\Gamma}_2$. These values are divided by the maximum value of the variance matrices used for simulation, to obtain a unit-free quantity. The errors for $\mathbf{\Gamma}_2$ are somewhat large, mirroring the conventional wisdom that estimating variance components requires quite a bit of data. In practice, using data from 35 subjects to estimate a 46 × 46 dimensional covariance matrix would not be advised. Even so, the drop in the mean squared errors from 35 to 70 and 70 to 140 subjects per group is only modest. Therefore, we recommend conservative interpretations of the covariance estimates when based on a limited sample size, relative to the total number of regions considered. However, in the Alzheimer's disease data set, we note that interesting results were obtained with 71 and 83 subjects in the two experimental groups, giving confidence that the covariance parameters were reasonably well-estimated. Also, additional information is obtained by comparing variance components representing bi-lateral and spatially contiguous structures. When limited sample sizes are available, an alternative is to reduce the number of regions considered, as was done in the cocaine-dependence study. The estimates of the residual variance, σ^2_{gj}, in the simulation study based on the Alzheimer's disease data were fairly good for all sample sizes considered. The median ratios of the estimates to the true value were 1.0152, 1.0146 and 1.0141 for the three sample sizes for $j = 1$ and 1.0147, 1.0138 and 1.0131 for $j = 2$. The λ^2_{gj} parameters tended to be poorly estimated for the sample sizes considered. For example, the median ratios to the true value for samples of size 70 were 0.08 and 0.10. This is to be expected, as even if the $\boldsymbol{\mu}_{gj}$ were known exactly, there would be considerable difficulty in estimating λ_{gj} for regions with few voxels.

6 Discussion

We propose a spatial Bayesian hierarchical model for analyzing functional neuroimaging data, which has several key advantages over alternative approaches. First, our model provides a unified framework to obtain neuroactivation inferences as well as task-related functional connectivity inferences, rather than treating these as distinct analytical objectives. Secondly, we may investigate neuroactivation at both the voxel level and at a regional level. It is important to note that the voxel-level inferences provided by our approach account for prominent long- and short-range correlations in the brain. Often, conducting an ROI analysis involves averaging the measured brain activity within the defined ROI, and then performing all subsequent analyses as though the data represent a single location. Two drawbacks of this approach are that it risks oversimplifying effects in ROI's that do not exhibit relatively uniform activity throughout, e.g. failing to identify significant activity in an ROI that is partially active. Moreover, these analyses use variance estimates of the ROI-averages that assume independence between voxels, when we would rarely expect such an assumption to hold in practice. Our approach overcomes these two limitations because our model retains voxel-specific estimates of changes in measured brain activity to detect partially activated regions, and our model accounts for the correlations between the parameters involved in the regional summaries.

Additional advantages of our model stem from our use of a Bayesian paradigm, which provides a range of flexible inferences. The Bayesian framework enables us to formulate probabilistic statements that help to quantify the evidence provided by our experimental data. The inference framework also allows us to compute credible intervals (or Bayesian confidence intervals) to make statistical inferences. Further, the MCMC estimation procedures produce samples from the joint posterior distribution of all of the model parameters, which facilitates estimation of and inferences about functions of the model parameters. In our fMRI examples, the intra-regional coherence (correlation) parameters served as particular examples that increased the interpretation content of our analyses. Despite the apparent complexity and rather rich formulation of our Bayesian hierarchical model as well as the high throughput nature of the data, computations for estimation are quite fast. For instance, estimation for the Bayesian hierarchical models for our two fMRI examples took less than 30 minutes each on a Linux cluster containing 4 processors with AMD Operton 850 CPUs (2.4Ghz) and 8GB RAM.

It is difficult to assess to what extent the estimated intra-regional correlations represent intrinsic factors, such as image resolution and preprocessing versus neurophysiologic connectivity within the region. Spatial smoothing of the data during preprocessing adds to the inability to differentiate between the source of intra-regional coherence. This issue is not unique to our setting and faces most other statistical methods that quantify functional connectivity based on the BOLD fMRI signal (in our case, summary statistics from the BOLD response). We refrained from spatial smoothing in our analyses. However, if smoothing seems important for a particular data set, e.g. to reduce the effect of high-frequency variation or to reduce individual variability in neuroanatomy, we recommend the use of a relatively small full width at half maximum and conservative interpretations of the intra-regional correlation estimates. Despite the potential influence of non-neurophysiologic factors on intra-regional correlations, our group-level analysis evaluating differences in estimated intra-regional connectivity between control and at-risk subjects in the Alzheimer's study should reflect actual differences in connectivity, since both groups were scanned and the resulting images preprocessed in a consistent manner.

We employ credible intervals, a likelihood-based tool, as the basis for our statistical inferences, and one may alternatively use Bayes factors. Each credible interval in our analyses is derived from samples from the joint posterior distribution of all of the model parameters. The question

of whether additional adjustments are necessary to cope with multiple testing is the source of ongoing debate. For example, some suggest that the use of the likelihood methods eliminates the need for multiple comparisons adjustments (Royall, 2000, 1997; Blume, 2002). For instance, Blume (2002) states that ”likelihood based methods permit the construction of any number of subgroups and allow for the evaluation of their evidence without adjustment,” in context of a clinical trial. Nonetheless, methods for Bayesian multiple testing procedures remains an active area of investigation (Berry and Hochberg, 1999; Efron and Tibshirani, 2002; Scott and Berger, 2006). Further research is required to resolve the question of whether the multiple testing is prudent for likelihood-based methods.

As illustrated in our simulation study, large sample sizes contribute to improved estimation of the model parameters. From a design perspective, one should attempt to employ large sample sizes to increase the accuracy of the estimates produced by our model. When large sample sizes are infeasible, one may alternatively limit the number of regions considered, which should be performed in line with the main research objectives.

Our analyses consider a particular neuroanatomic parcellation of the brain into distinct regions (Tzourio-Mazoyer et al., 2002), but other such parcellations, for example based on Brodmann area maps or the Freesurfer software (Fischl et al., 2004, 2002) are available. As an alternative to neuroanatomic approaches, one may also use data-driven segmentation procedures such as functional clustering (Bowman and Patel, 2004; Cordes et al., 2002). One potential advantage of using data-driven techniques that pool voxels with similar activity profiles into regions or clusters is that this approach may contribute favorably to support the model assumption of exchangeable covariance structures within each region. However, a notable drawback is that data-driven approaches often produce clusters (or regions) that are more difficult to interpret than the neuroanatomically defined regions. A combination of these two general approaches could also be employed by applying data-driven segmentation procedures within each anatomically defined region.

We formulate our spatial model by building on the commonly applied two-stage approach, in which temporal correlations are primarily addressed in the first stage. Given our Bayesian model formulation presented here, an area of future research involves examining the feasibility of combining the two stages into a unified spatio-temporal model. Although conceptually simple, a detailed investigation is necessary to develop, implement, and validate such a modeling approach.

Acknowledgments

The work of Bowman was supported by the National Institute of Mental Health (NIH grants K25-MH65473 and R01-MH079251). The work of Bassett and Caffo was supported by NIH grants AG016324 and EB003491.

References

Albert P, McShane L. A generalized estimating equations approach for spatially correlated binary data: Applications to the analysis of neuroimaging data. Biometrics 1995;51:627–638. [PubMed: 7662850]

Aron AR, Poldrack RA. Cortical and Subcortical Contributions to Stop Signal Response Inhibition: Role of the Subthalamic Nucleus. J. Neurosci 2006;26:2424–2433. [PubMed: 16510720]

Bassett S, Yousem D, Christinzio C, Kusevic I, Yassa M, Caffo B, Zeger S. Familiar riks for alzheimer's disease alters fMRI activation patterns. Brain 2006;129:1229–1239. [PubMed: 16627465]

Berry DA, Hochberg Y. Bayesian perspectives on multiple comparisons. Journal of Statistical Planning and Inference 1999;82:215–277.

Blasi G, Goldberg TE, Weickert T, Das S, Kohn P, Zoltick B, Bertolino A, Callicott JH, Weinberger DR, Mattay VS. Brain regions underlying response inhibition and interference monitoring and suppression. European Journal of Neuroscience 2006;23(6):1658–1664. [PubMed: 16553630]

Blume JD. Tutorial in biostatistics: Likelihood methods for measuring statistical evidence. Statistics in Medicine 2002;21:2563–2599. [PubMed: 12205699]

Bookheimer S, Strojwas M, Cohen M, Saunders A, Pericak-Vance M, Mazziotta J, Small G. Patterns of brain Activation in people at risk for alzheimer's disease. New England Journal of Medicine 2000;343:450–456. [PubMed: 10944562]

Bowman F. Spatiotemporal modeling of localized brain activity. Biostatistics 2005;6:558–575. [PubMed: 15843592]

Bowman F. Spatio-temporal models for region of interest analyses of functional neuroimaging data. Journal of the American Statistical Association. 2007

Bowman FD, Patel R. Identifying spatial relationships in neural processing using a multiple classification approach. NeuroImage 2004;23:260–268. [PubMed: 15325373]

Cordes D, Haughton V, Carew J, Arfanakis K, K M. Hierarchical clustering to measure connectivity in fmri resting state data. Magn Reson Imag 2002;20:305–317.

Efron B, Tibshirani R. Empirical bayes methods and false discovery rates for microarrays. Genetic Epidemiology 2002;23:70–86. [PubMed: 12112249]

Fischl B, Salat D, Busa E, Dieterich M, Haselgrove C, Van der Kouwe A, Killiany R, Kennedy D, Klaveness S, Montillo A, Makris N, Rosen B, Dale A. Whole brain segmentation: Automated labeling of neuroanatomical structures in the human brain. Neuron 2002;33:341–355. [PubMed: 11832223]

Fischl B, Van der Kouwe A, Destrieux C, Halgren E, Segonne F, Salat D, Busa E, Seidman L, Goldstein J, Kennedy D, Caviness V, Makris N, Rosen B, Dale A. Automatically parcellating the human cerebral cortex. Cerebral Cortex 2004;14:11–22. [PubMed: 14654453]

Friston K, Frith C, Liddle P, Frackowiak R. Functional connectivity: the principal-component analysis of large (PET) data sets. Journal of Cerebral Blood Flow and Metabolism 1993;13:5–14. [PubMed: 8417010]

Friston K, Holmes A, Worsley K, Poline J, Frith C, Frackowiak R. Statistical parametric maps in functional imaging: A general linear approach. Human Brain Mapping 1995;2(189–210)

Friston K, Penny W, Phillips C, Kiebel S, Hinton G, Ashburner J. Classical and Bayesian inference in neuroimaging: theory. NeuroImage 2002;16(465–483)

Garavan H, Ross TJ, Murphy K, Roche RAP, Stein EA. Dissociable executive functions in the dynamic control of behavior: Inhibition, error detection, and correction. NeuroImage 2002;17:1820–1829. [PubMed: 12498755]

Garey, L. Brodman's localisation in the cerebral cortex: the principles of comparative localisation based on cytoarchitectonics. Springer; London: 1994. English translation of Vergleichende Lokalisationslehre der Grosshirnrinde by Korbinian Brodman

Gössl C, Auer D, Fahrmeir L. Bayesian spatiotemporal inference in functional magnetic resonance imaging. Biometrics 2001;57:554–562. [PubMed: 11414583]

Hampson M, Peterson B, Skudlarski P, Gatenby J, Gore J. Detection of functional connectivity using temporal correlations in MR images. Human Brain Mapping 2002;15:247–262. [PubMed: 11835612]

Holmes A, Blair R, G W, Ford I. Nonparametric analysis of statistic images from functional mapping experiments. Journal of Cerebral Blood Flow and Metabolism 1996;16:7–22. [PubMed: 8530558]

Jones G, Haran M, Caffo B, Neath R. Fixed-width output analysis for Markov chain Monte Carlo. Journal of the American Statistical Association 2006;101:1537–1547.

Kalivas P, Volkow n. The neural basis of addiction: A pathology of motivation and choice. American Journal of Psychiatry. 2005

Katanoda K, Matsuda Y, Sugishita M. Spatio-temporal regression model for the analysis of functional MRI data. NeuroImage 2002;17:1415–1428. [PubMed: 12414281]

Kiebel, S. The general linear model.. In: Frackowiak, R.; Friston, K.; Frith, C.; Dolan, R.; Friston, K.; Price, C.; Zeki, S.; Ashburner, J.; Penny, W., editors. Human Brain Function. 2nd edition. Academic Press; 2003.

Konishi S, Nakajima K, Uchida I, Kikyo H, Kameyama M, Miyashita Y. Common inhibitory mechanism in human inferior prefrontal cortex revealed by event-related functional MRI. Brain 1999;122:981–991. [PubMed: 10355680]

Mardia, K.; Kent, J.; Bibby, J. Multivariate Analysis. Academic Press; San Diego: 1979.

Matsumoto R, Nair D, LaPresto E, Najm I, Bingaman W, Shibasaki H, Lüders H. Functional connectivity in the human language system: a cortico-cortical evoked potential study. Brain 2004;127:2316–2330. [PubMed: 15269116]

Patel N, Bowman F, Rilling J. A bayesian approach to determining connectivity of the human brain. Human Brain Mapping 2006a;27:267–276. [PubMed: 16092131]

Patel N, Bowman F, Rilling J. Determining hierarchical functional networks from auditory stimuli fMRI. Human Brain Mapping 2006b;27:462–470. [PubMed: 16568419]

Penny W, Trujillo-Barreto N, Friston K. Bayesian fMRI time series analysis with spatial priors. NeuroImage 2005;24:350–362. [PubMed: 15627578]

Royall, RM. Statistical Evidence: A Likelihood Paradigm. Chapman and Hall; London: 1997.

Royall RM. On the probability of observing misleading statistical evidence. Journal of the American Statistical Association 2000;95:760–768.

Rubia K, Taylor E, Smith AB, Oksannen H, Overmeyer S, Newman S. Neuropsychological analyses of impulsiveness in childhood hyperactivity. Br J Psychiatry 2001;179(2)

Scott JG, Berger JO. An exploration of aspects of bayesian multiple testing. Journal of Statistical Planning and Inference 2006;136:2144–2162.

Tadesse M, Ibrahim J, Vannucci M, Gentleman R. Wavelet thresholding with bayesian false discovery rate control. Biometrics 2005;61(1):25–35. [PubMed: 15737075]

Tzourio-Mazoyer N, Landeau B, Papathanassiou D, Crivello F, Etard O, Delcroix N, Mazoyer B, M J. Automated anatomical labeling of activations in SPM using a macroscopic anatomical parcellation of the MNI MRI single-subject brain. NeuroImage 2002;15:273–289. [PubMed: 11771995]

West, M.; Harrison, J. Applied Bayesian forecasting and time series analysis. Chapman and Hall / CRC; Boca Raton: 1989.

Woolrich M, Behrens T, Smith S. Constrained linear basis sets for HRF modelling using variational Bayes. NeuroImage 2004a;21:1748–1761. [PubMed: 15050595]

Woolrich M, Jenkinson M, Brady J, Smith S. Fully Bayesian spatio-temporal modeling of fMRI data. IEEE Transactions on Medical Imaging. 2004b

Worsley K. Local maxima and the expected Euler characteristic of excursion sets of χ^2, F, and t fields. Advances in Applied Probability 1994;26:13–42.

Worsley K, Evans A, Marrett S, Neelin P. A three-dimensional statistical analysis for rCBF activation studies in the human brain. Journal of Cerebral Blood Flow and Metabolism 1992;12:900–918. [PubMed: 1400644]

Worsley K, Evans A, Strother S, Tyler J. A linear spatial correlation model, with applicability to positron emission tomography. Journal of the American Statistical Association 1991;86:55–67.

Worsley K, Liao C, Aston J, Petre V, Duncan G, Moralese F, Evans A. A general statistical analysis for fMRI data. NeuroImage 2002;15:1–15. [PubMed: 11771969]

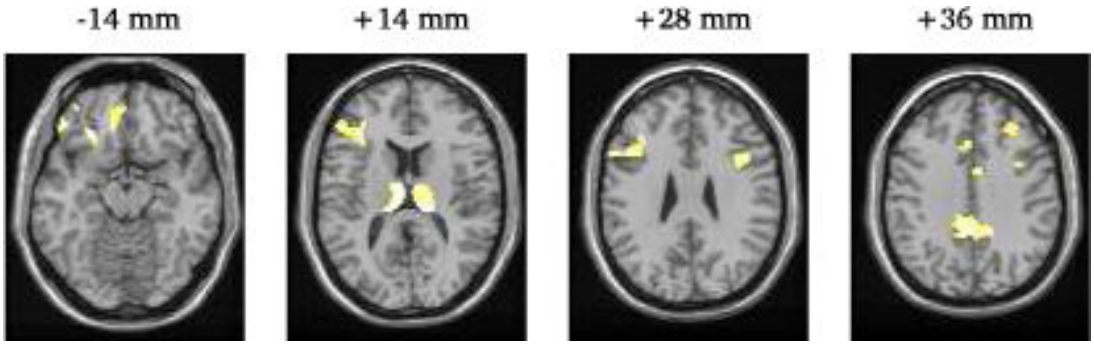

Figure 1.
The maps portray voxel-specific posterior probabilities, exceeding 0.80, of increased activity from baseline to the post-treatment period for the cocaine addicts, relative to (minus) the corresponding baseline-to-follow-up differences in the control subjects. The axial slices are at various distances (in millimeters (mm)) from the anterior-posterior commissural plane. The activations include the medial orbital frontal cortex (BA 11) [at −14 mm], the left middle frontal gyrus (BA 46) and left and right thalamus [at +14 mm], bilaterally in the middle frontal gyrus (BA 9) [at +28 mm], and along the cingulate gyrus (BA 31, 32), with the posterior cingulate activation appearing more spatially extensive [at +36].

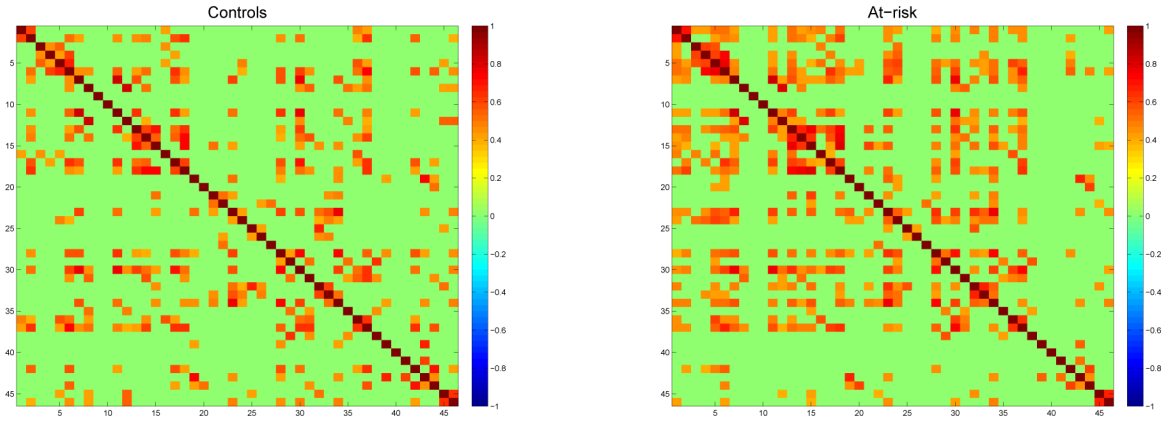

Figure 2.
Posterior mean estimates of inter-regional connectivity for the Alzheimer's disease data set. Corresponding region names and indices are given in Table 1.

Table 1

Posterior mean and credible interval (CI) estimates of regional correlations for the 46 regions of interest considered in the Alzheimer's disease study. Notation is as follows, R=right, L=left, Ctr = Control, AR = At-risk, A = Anterior, Cau = Caudate, Cing = cingulum, Fr = frontal, He = Heschl gyrus, Hippo = hippocampus, Inf=inferior, Med = medial, Mid=middle, OF=orbital frontal, Op = Operculum, Pal = Pallidum, Pc = Postcentral gyrus, PHG = Parahippocampal gyrus, Pr = precentral gyrus, Rol = Rolandic, SMA = Supplementary motor area, SMG = Supra-marginal gyrus, Sup = Superior, Thal = Thalamus, Temp = Temporal gyrus, TP = Temporal pole, Tr = Triangularis.

	Region	Ctr	AR	CI		Region	Ctr	AR	CI
1	L Cau	0.30	0.27	[0.86, 1.43]	24	R Insula	0.13	0.17	[0.58, 1.08]
2	R Cau	0.38	0.35	[0.84, 1.34]	25	L Pal	0.34	0.34	[0.77, 1.26]
3	L A Cing	0.18	0.26	[0.52, 0.92]	26	R Pal	0.30	0.30	[0.76, 1.29]
4	R A Cing	0.16	0.26	[0.47, 0.84]	27	R PHG	0.61	0.60	[0.87, 1.18]
5	L Mid Cing	0.16	0.22	[0.53, 0.98]	28	L Po	0.32	0.36	[0.68, 1.11]
6	R Mid Cing	0.20	0.26	[0.59, 1.04]	29	R Po	0.25	0.27	[0.72, 1.23]
7	L Inf Op Fr	0.22	0.27	[0.61, 1.07]	30	L Pr	0.19	0.22	[0.66, 1.18]
8	R Inf Op Fr	0.18	0.20	[0.68, 1.23]	31	R Pr	0.19	0.15	[0.95, 1.75]
9	L Inf OF	0.57	0.63	[0.78, 1.06]	32	L Put	0.31	0.31	[0.76, 1.28]
10	R Inf OF	0.37	0.41	[0.72, 1.12]	33	R Put	0.31	0.29	[0.84, 1.40]
11	L Inf Tr Fr	0.21	0.27	[0.60, 1.05]	34	L Rol Op	0.25	0.27	[0.72, 1.24]
12	R Inf Tr Fr	0.18	0.26	[0.54, 0.96]	35	R Rol Op	0.18	0.19	[0.70, 1.27]
13	L Mid Fr	0.17	0.20	[0.65, 1.17]	36	L SMA	0.19	0.20	[0.71, 1.28]
14	R Mid Fr	0.19	0.19	[0.72, 1.30]	37	R SMA	0.25	0.26	[0.73, 1.24]
15	L Sup Fr	0.23	0.33	[0.54, 0.92]	38	R SMG	0.50	0.48	[0.87, 1.26]
16	L Sup Med Fr	0.23	0.23	[0.75, 1.32]	39	L Mid Temp	0.51	0.54	[0.80, 1.14]
17	R Sup Med Fr	0.32	0.36	[0.69, 1.12]	40	R Mid Temp	0.48	0.45	[0.86, 1.33]
18	R Sup Fr	0.27	0.34	[0.62, 1.03]	41	L Sup TP	0.35	0.36	[0.77, 1.23]
19	L He	0.48	0.42	[0.94, 1.41]	42	R Sup TP	0.50	0.45	[0.91, 1.33]
20	R He	0.27	0.30	[0.70, 1.17]	43	L Sup Temp	0.28	0.27	[0.81, 1.37]
21	L Hippo	0.38	0.47	[0.65, 1.00]	44	R Sup temp	0.23	0.18	[0.94, 1.69]
22	R Hippo	0.40	0.38	[0.85, 1.33]	45	L Thal	0.13	0.17	[0.58, 1.10]
23	L Insula	0.20	0.21	[0.71, 1.28]	46	R Thal	0.15	0.17	[0.66, 1.23]